frontiers | Frontiers in Earth Science

TYPE Original Research
PUBLISHED 05 April 2023
DOI 10.3389/feart.2023.1057936

OPEN ACCESS

EDITED BY
Sarah Jaye Oliva,
University of Victoria, Canada

REVIEWED BY
Dongliang Liu,
Institute of Geology, Chinese Academy of Geological Sciences (CAGS), China
Chen Wu,
Chinese Academy of Sciences (CAS), China

*CORRESPONDENCE
Xuanhua Chen,
xhchen@cags.ac.cn

SPECIALTY SECTION
This article was submitted to Structural Geology and Tectonics, a section of the journal Frontiers in Earth Science

RECEIVED 30 September 2022
ACCEPTED 15 March 2023
PUBLISHED 05 April 2023

CITATION
Wang Y, Chen X, He C, Xiao Y, Shao Z, Han J, Li B, Zhang Y, Ding W, Xu S and Han L (2023), Active tectonics and paleo-earthquakes in north Yumu Shan, northern Tibetan Plateau: Insights from structural analysis and radiocarbon dating.
Front. Earth Sci. 11:1057936.
doi: 10.3389/feart.2023.1057936

Active tectonics and paleo-earthquakes in north Yumu Shan, northern Tibetan Plateau: Insights from structural analysis and radiocarbon dating

Ye Wang[1], Xuanhua Chen[1]*, Chengguang He[2], Yongjun Xiao[3], Zhaogang Shao[1], Jian'en Han[4], Bing Li[1], Yiping Zhang[1], Weicui Ding[1], Shenglin Xu[1] and Lele Han[1,5]

[1]SinoProbe Center, Chinese Academy of Geological Sciences and China Geological Survey, Beijing, China, [2]Henan Institute of Geological Survey, Zhengzhou, China, [3]Research Institute of Petroleum Exploration and Development, Sinopec Shengli Oilfield Company, Dongying, Shandong, China, [4]Institute of Geomechanics, Chinese Academy of Geological Sciences, Beijing, China, [5]School of Earth Sciences and Resources, China University of Geosciences (Beijing), Beijing, China

The Yumu Shan is located at the northern margin of the Tibetan Plateau in northwest China. It is characterized by the development of several northeastward-protruding arcuate geomorphic bulge belts on its north slope. These bulge belts are distributed along the Wutongquan spring, the ancient Camel City, and the Xiaogengzi area, and south to Gaotai City in the Hexi Corridor. In this study, our detailed field mapping and structural analysis reveal northeastward active anticline folding along the curved bulge belts and related lacustrine sediments in their hinterlands. Radiocarbon dating of plant charcoal samples from lacustrine sedimentary layers yields a ^{14}C age of AD 178 $\pm$ 42. This age is close to the time of the 180AD/Ms7.5 earthquake at Biaoshi City (i.e., the ancient Zhangye City) during the Eastern Han Dynasty. The similarity between seismic events and sedimentary age leads us to infer that the charcoal in the lacustrine layer records a major flood event related to the Biaoshi earthquake. We propose a fault-related fold model for the formation of the arcuate bulge belts and related sediments. First, a series of historical earthquake activities in the Holocene, especially the 180AD/Ms7.5 Biaoshi earthquake, may have led to active blind thrust faulting in the northern margin of the plateau. Then, blind thrusting may have resulted in fault-related anticline folding, causing the formation of geomorphic bulges. The latter acts as a flood-retaining dam, resulting in hinterland deposition of lacustrine sediments. For this reason, we suggest that seismogenic blind thrust faulting is responsible for the uplift and northward growth of the Tibetan Plateau. As the northernmost blind thrust in this area, the Xiaogengzi Fault could be considered the North Boundary Thrust (NBT), which defines exactly the northern margin of the plateau.

KEYWORDS

active tectonics, paleo-earthquake, radiocarbon dating, blind thrusts, plateau growth, Hexi Corridor, northeast Tibet

Introduction

The most significant consequence of the continental Indo-Asian collision in the Cenozoic was the formation of the Himalayan–Tibetan orogen and the growth of the Tibetan Plateau due to the ongoing penetration of the Indian plate into the Eurasian plate (Tapponnier et al., 1982; Tapponnier et al., 1986; Royden et al., 1997; Clark and Royden, 2000; Yin and Harrison, 2000; Yin, 2006; Royden et al., 2008; Yin, 2010; Wang et al., 2014; Chen et al., 2022a; Gao et al., 2022). As a far-field response to the collision, the Cenozoic Qilian Shan–Nan Shan (Shan means "mountain" in Chinese) fold-and-thrust belt formed in the northern Tibetan Plateau (Yin et al., 2002; Yin et al., 2008a; Yin et al., 2008b; Chen et al., 2010; Zhang et al., 2017; Cheng et al., 2021), leading to the formation of the Hexi Corridor as its foreland basin. Some studies have proposed that the collision between the Lhasa and Qiangtang terranes from the latest Jurassic to the earliest Cretaceous time may have played an important role in the formation of the northern Tibet Plateau (Coward et al., 1988; Harris et al., 1988; Kidd and Molnar, 1988). Recently, our study revealed Mesozoic deformation, especially Early Cretaceous compressional deformation, significantly controlled the Cenozoic evolution of the northern Qilian Shan (e.g., Chen et al., 2019b; Li et al., 2021; Wu et al., 2021; Wang et al., 2022). At the northern margin of the plateau, many modern earthquakes occurred in the junction region between the Qilian Shan and the Hexi Corridor (Molnar, 1988; Zhang et al., 2004; Sukhija et al., 2006). However, the characteristics of active crustal deformation and the assessment of strong earthquakes remain in dispute in this region (Yu et al., 2021).

The identification of seismogenic faults of large historic earthquakes has great significance for determining seismic mechanisms and faulting behaviors in regions experiencing active tectonic deformation (Huntington et al., 2006; Chen et al., 2021). The Yumu Shan region is a major and seismically active thrust belt located at the junction of the Qilian Shan and the Hexi Corridor in the northern Tibetan Plateau (Chen et al., 2019a). It is considered to be the northward-expanding front of the Tibetan Plateau and is characterized by steep tectonic relief (Chen et al., 2022b). Previous research has revealed that the region suffered multi-phase deformations in the Mesozoic and Cenozoic (Vincent and Allen, 1999; Chen et al., 2019a; Wang et al., 2022), especially intensive folds and thrusts formed in the Quaternary (Tapponnier et al., 1990; Chen et al., 2006; Chen et al., 2008; Yang et al., 2018a; Yang et al., 2018b; Ren et al., 2019). Major active thrust faults around the Yumu Shan play an important role in releasing the strain energy accumulated during the Indo-Asian collision and the formation of large earthquakes. Therefore, the Yumu Shan region provides an excellent natural laboratory in which to study active deformation in an intraplate seismic environment.

In this study, we conducted systematically detailed geological mapping and structural analysis in the field to determine the Cenozoic deformational pattern of folding and blind thrusting in the Yumu Shan region of the northern Tibetan Plateau (Figure 1). We adopted radiocarbon dating of plant charcoal samples to test potential links between the notorious 180AD/Ms7.5 Biaoshi earthquake during the Eastern Han Dynasty, blind thrusting along the Xiaogengzi Fault, and lacustrine sedimentation.

Geological setting

The Qilian Shan is an Early Paleozoic orogen and reactivated the Cenozoic fold-and-thrust belt along the northern margin of the Tibetan Plateau in the northernmost part of the Tethys regime (Figure 1; Yin and Harrison, 2000; Xiao et al., 2009; Yin, 2010; Song et al., 2014; Li et al., 2018; Zuza et al., 2018; Zuza et al., 2019; Li et al., 2019; Li et al., 2020; Chen et al., 2019a; Chen et al., 2022a; Wu et al., 2021; Cheng et al., 2021; Gao et al., 2022). It is bounded by the left-lateral strike–slip Altyn Tagh fault, the North Qaidam fault, and the North Qilian fault (NQLF). The left-lateral strike–slip Haiyuan fault and the Tianjingshan fault together define the northeastern marginal zone of the Qilian Shan. These two left-slipping faults are kinematically connected to the WNW-striking thrust fault system in the hinterland of the Qilian Shan to the west and in the NNW-striking Liupanshan thrust to the east. The Early Paleozoic Qilian orogen has experienced the subduction of the North Qilian Ocean and collisional orogeny between the East Kunlun–Qaidam–Central Qilian and Tarim–North China blocks (Gao et al., 2022). During the Indo-Asian continental collision in the Cenozoic, the Qilian Shan served as the northernmost front of the Tibetan Plateau (Wang et al., 2014). The uplift of the Qilian Shan was due to the continuous extrusion of the Tibetan Plateau (Métivier et al., 1998; Meyer et al., 1998; Tapponnier et al., 2001). The cooling history of the northern Qilian Shan (20~10 Ma, George et al., 2001; 17~15 Ma; Yu et al., 2019) shows exhumation and northeastward expanding in the northern margin of the plateau since the Miocene.

The Hexi Corridor is a major seismically active belt in northwestern China. It is an elongated basin located between the Qilian Shan in the south and the Alxa Terrane in the north. The Hexi Corridor basin is bounded by the NQLF to the south and the Longshoushan fault to the north (Figure 2). Generally, it is considered the foreland basin of the Qilian Shan and the northernmost expansional front of the Tibetan Plateau (Tapponnier et al., 1990; Li et al., 1999; Hetzel et al., 2004; Chen et al., 2006; 2008; Zhang et al., 2017; Yang et al., 2018a; Yang et al., 2018b). Previous studies have revealed a south-dipping blind thrust (i.e., the Kuantanshan Fault) in the Jiayuguan, west of the Hexi Corridor. The fault is considered the North Boundary Thrust (NBT) of the Tibetan Plateau in that region (Gao et al., 1998). North to the Hexi Corridor, the north-dipping South Heli Shan thrust leads to the uplift of the Heli Shan during 4–1 Ma (or since ca. 2 Ma), implying that the northeastward expansion of the Tibetan Plateau may have crossed over the Hexi Corridor to the north (Zheng et al., 2013).

Between the Qilian Shan and the Hexi Corridor, the Yumu Shan is a locally high elevation and a key junction zone for understanding the uplift and northeastward expansion of the Tibetan Plateau (Figure 2; Chen et al., 2017; Yang et al., 2018a; Yang et al., 2018b; Chen et al., 2019b). It is also a boundary separating the Hexi Corridor basin from the Jiuquan Basin in the west and the Minle Basin in the east (Figure 2). Recently, an earlier Early Cretaceous large-scale thrust and nappe system was recognized in

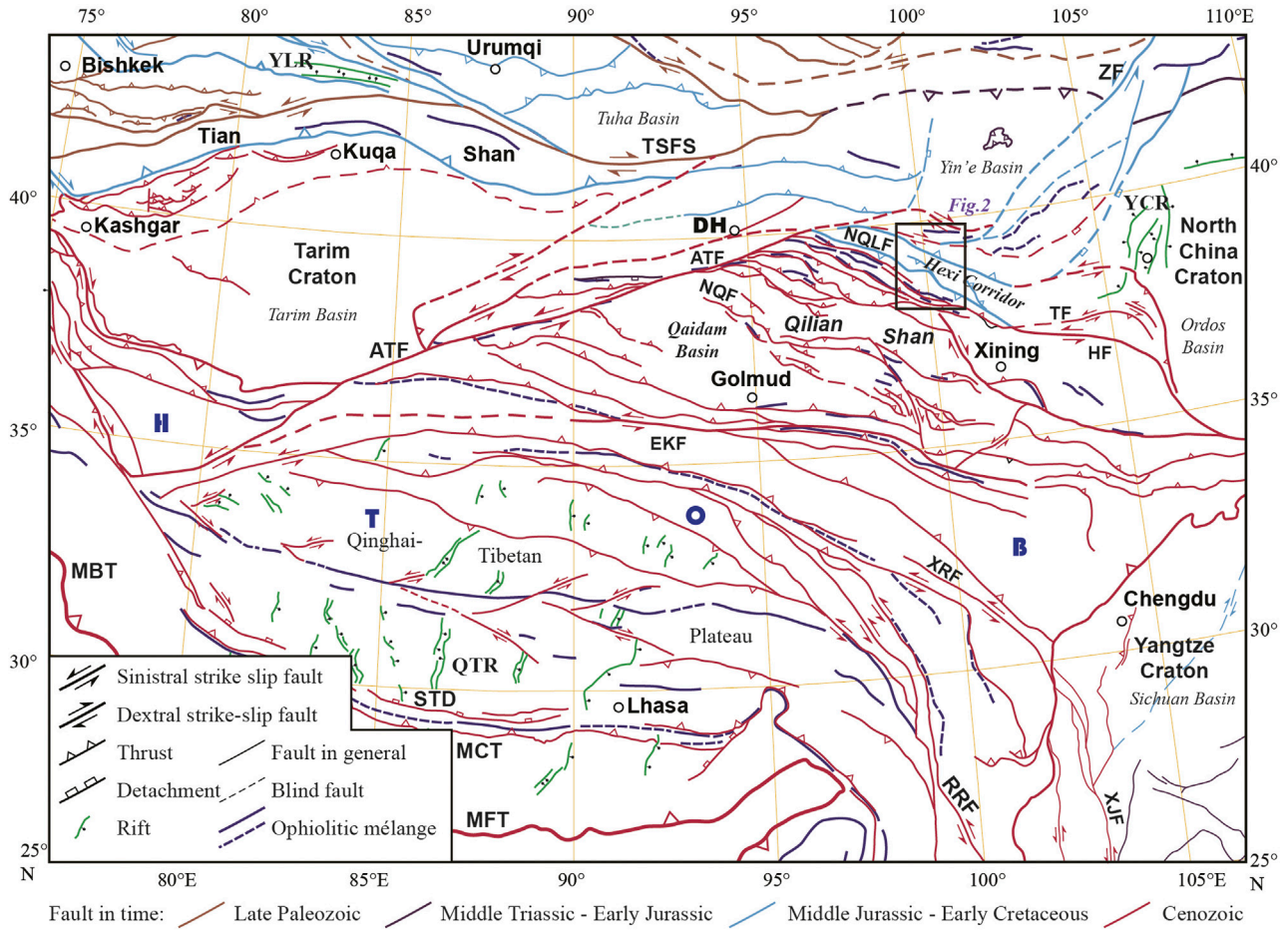

FIGURE 1
Simplified fault system of the Tibetan Plateau, modified from Yin et al. (2008a), Yin et al. (2008b), Chen et al. (2019a), and Chen et al. (2022a). HTOB, Himalaya–Tibetan Orogenic Belt. Faults: ATF, Altyn Tagh; NQLF, North Qilian; NQF, North Qaidam; HF, Haiyuan; TF, Tianjingshan; ZF, Zuunbayan; RRF, Red River; XRF, Xianshui River; EKF, East Kunlun. TSFS, Tianshan strike–slip fault system. STD, South Tibet Detachment; MCT, Main Central Thrust; MBT, Main Boundary Thrust; MFT, Main Frontal Thrust. Rift systems: YCR, Yinchuan; YLR, Yili; QTR, Qinghai–Tibetan. DH, City of Dunhuang. The rectangle shows the location of Figure 2.

the Yumu Shan and its surrounding region, with the North Qilian Fault (NQLF) as the root zone of the system (Chen et al., 2019b). The development of later Early Cretaceous right-lateral strike–slip faulting and extensional graben basins confirms the formation of the Yumu Shan thrust and nappe system (YMTS) in the earlier Early Cretaceous, as a far-field response to the Lhasa–Qiangtang collision in the south (Wang et al., 2022).

The Yumu Shan is occupied mainly by Silurian flysch formations of graywackes, siltstones, and slates (Figure 2; Chen et al., 2019b). Devonian volcanic and pyroclastic rocks, conglomerates, and glutenites are locally exposed in the Yumu Shan and its surrounding areas. The Permian is composed of glutenites, sandstones, calcareous sandstones, siltstones, and black mudstones outcropping south to the Yumu Shan. The Triassic sandstones, siltstones, and slates, and the Lower Jurassic conglomerates, sandstones, shales, and coal seams are sporadically and locally exposed. The Cretaceous, Neogene, and Quaternary strata are widely exposed in the peripheral zones of the Yumu Shan. The Cretaceous is characterized by purplish-red conglomerates, sandstones, argillaceous siltstones, mudstones, and marls, and by local outcrops of basaltic andesites and tuffaceous sandstones. The Neogene consists of pebbly sandstones, argillaceous siltstones, sandy mudstones, and marlites. The Quaternary comprises alluvial–proluvial, aeolian, lacustrine, swamp, and chemical deposits, and moraine conglomerates of the Yumen Formation (Figure 3; BGGP, 1971; BGGP, 1973).

Magmatic plutons are not popular in the Yumu Shan and surrounding area. There are some small-sized Early Paleozoic granitoid intrusions outcropping in the Jinyaosi area south to the Yumu Shan (Figure 2). Some small-sized Devonian syenogranite intrusions occur in the Silurian and Devonian strata in the Yumu Shan area (Figure 3; BGGP, 1971; BGGP, 1973).

Structural analyses

The fieldwork described in this study primarily focused on regional geological surveying and thematic structural geological

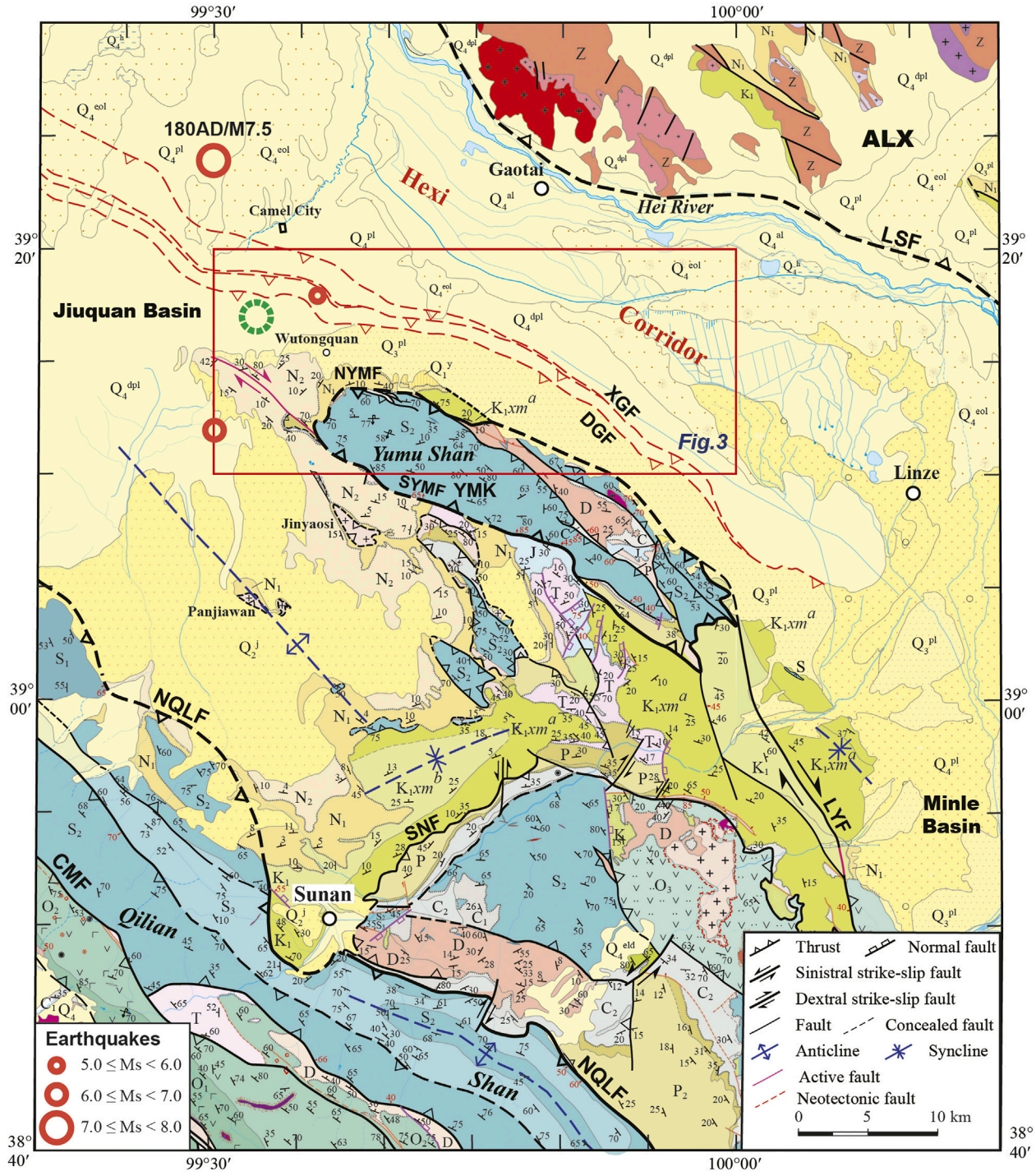

FIGURE 2
Geological map of the Yumu Shan and surrounding region in northern Qilian Shan and Hexi Corridor, modified from Chen et al. (2019b) and Wang et al. (2022). Locations of earthquake events are from Ren et al. (2019). The green dashed circle shows our suggested location for the 180AD/Ms7.5 Biaoshi earthquake. ALX, Alxa block. Q_h, Holocene. Q_p, Pleistocene. N_2, Pliocene. N_1, Miocene. E, Paleogene. K_1, Lower Cretaceous. J, Jurassic. T, Triassic. P, Permian. C_2 and C_1, Upper and Lower Carboniferous. D, Devonian. S_3, S_2, and S_1, Upper, Middle, and Lower Silurian. O_3, O_2, and O_1, Upper, Middle, and Lower Ordovician. CMF, Changma Fault. NQLF, North Qilian Fault. NYMF, North Yumu Shan Fault. SYMF, South Yumu Shan Fault. LSF, Longshoushan Fault. LYF, Liyuanpu Fault. SNF, Sunan Fault. DGF, Dagengzi Fault. XGF, Xiaogengzi Fault. YMK, Yumu klippe. The location of Figure 3 is represented with a red rectangle.

mapping of key locations in the northern Qilian Shan and the Hexi Corridor using Google Earth image interpretation, strata relationship and tectonic relief comparison, structural analysis, and growth strata determination (Chen et al., 2019a; Chen et al., 2019b; Wang et al., 2020; Chen et al., 2022b; Wang et al., 2022). Our results reveal the multi-stage tectonic deformation that developed in

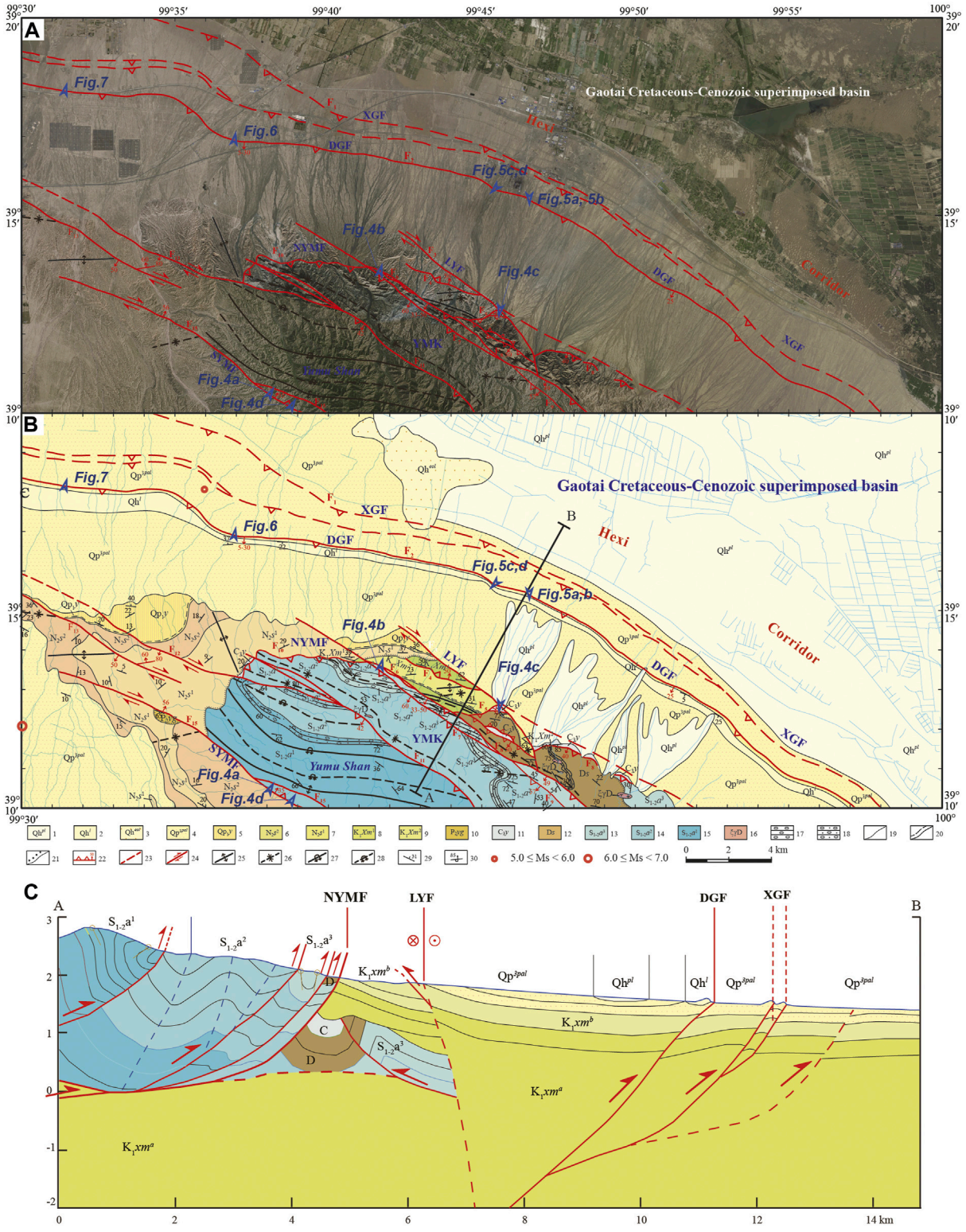

FIGURE 3
(A) Google Earth image of northern Yumu Shan. **(B)** Geological map of northern Yumu Shan based on our field observations. Modified from Chen et al. (2019b) and (Wang et al., 2022). Historical earthquake events are from Ren et al. (2019). Legends: 1—Holocene diluvial deposits; 2—Holocene lacustrine sediments; 3—Holocene aeolian sediments; 4—alluvial–pluvial deposits of the Upper Pleistocene; 5—Lower Pleistocene Yumen Formation; 6 and 7—upper and lower members of the Neogene Shulehe Formation; 8 and 9—upper and lower subgroups of the Lower Cretaceous Xinminpu Group; 10—Middle Permian Yaogou Formation; 11—Upper Carboniferous Yanghugou Formation; 12—Devonian Shaliushui Formation; 13, 14, and 15—third, second, and first members of the Middle-Lower Silurian; 16—Devonian syenogranite; 17—conglomerate; 18—sand conglomerate; 19—geological boundary; 20—parallel unconformity; 21—angular unconformity; 22—thrust fault; 23—blind fault; 24—strike–slip fault; 25—anticline; 26—syncline; 27—overturned anticline; 28—overturned syncline; 29—bedding; 30—overturned bedding. Locations of Figures 4A–D–4D, 5A–D–5D, 6, 7 are shown as rectangles. **(C)** Geological cross section (profile A–B) from the Yumu Shan to the Hexi Corridor.

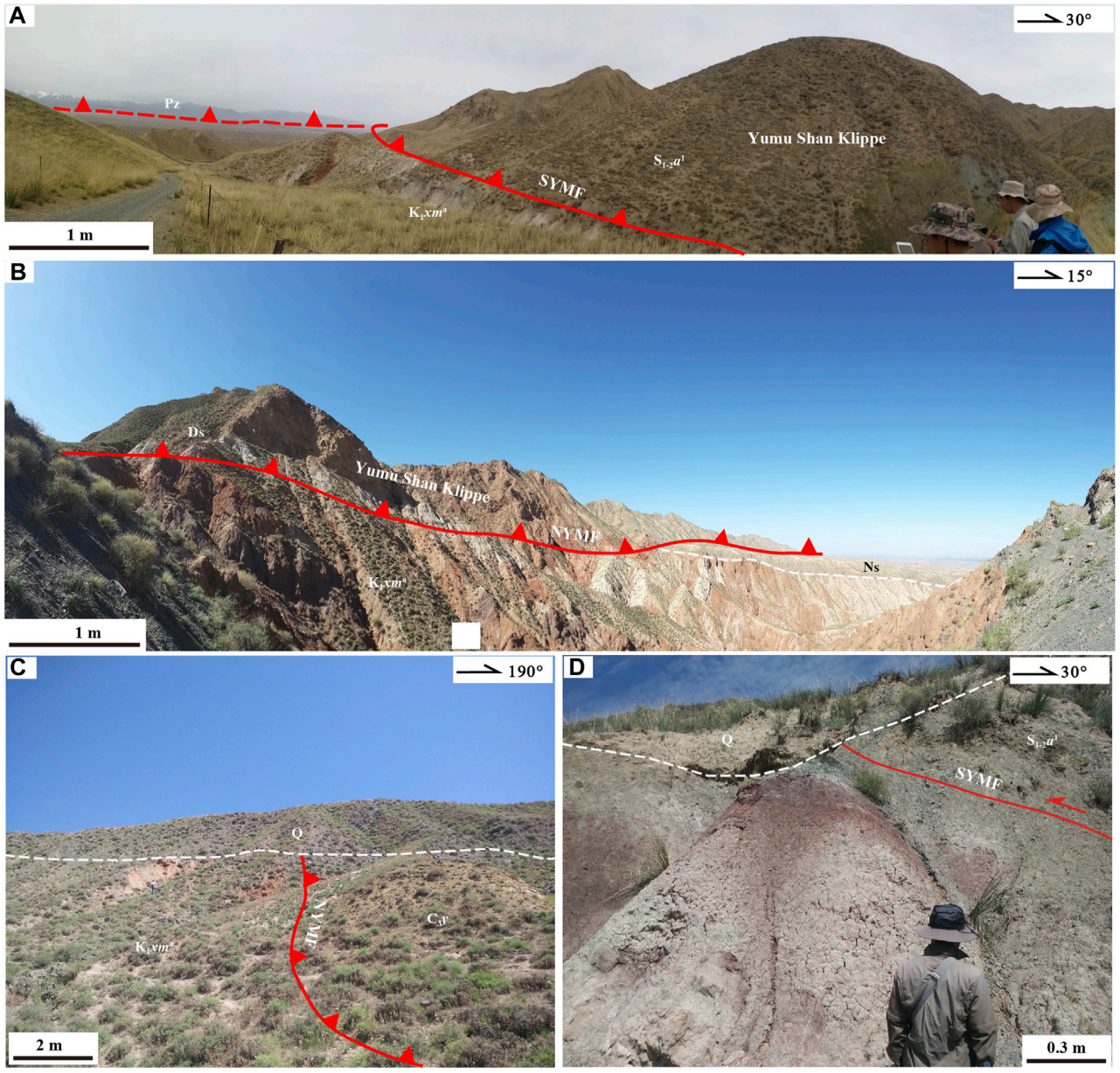

FIGURE 4
Field photographs from the Yumu Shan region, displaying contacts between the Lower Cretaceous (K_1) and overlying sequences. Photograph locations are shown in Figure 3. **(A)** SYMF placing the Silurian system ($S_{1\text{-}2}$) over the Lower Cretaceous strata (K_1). Pz, Paleozoic strata in north Qilian Shan. **(B)** NYMF placing the Silurian system ($S_{1\text{-}2}$) over the Lower Cretaceous strata (K_1) and unconformably covered by Neogene strata (N). **(C)** NYMF placing the Carboniferous strata (C_3) over the Lower Cretaceous strata (K_1) and unconformably covered by Quaternary strata (Q). **(D)** SYMF placing the Silurian system ($S_{1\text{-}2}$) over the Lower Cretaceous strata (K_1) and unconformably covered by Quaternary strata (Q).

the northern margin of the Tibetan Plateau, including the YMTS and the active fault system (Figures 2, 3).

The Yumu Shan thrust and nappe system (YMTS)

The YMTS is mainly composed of a series of NW- and NWW-striking thrust faults, folds, and klippes, including the NQLF, the Su'nan Fault, the South Yumu Shan Fault (SYMF), and the North Yumu Shan Fault (NYMF) (Figure 2; Chen et al., 2019b).

The root zone of the YMTS is located at the Fodongmiao–Hongyazi–Su'nan segment of the NQLF, which forms the northernmost front of the Qilian Shan. As the main thrust fault, the NQLF developed in the earlier Early Cretaceous and was reactivated in the Cenozoic (Chen et al., 2019b; Wang et al., 2022). It controlled the deposition of the Jiuquan Basin in the earlier Early Cretaceous.

The middle zone of the YMTS developed between the NQLF and the SYMF. Deep seismic reflection profiling reveals that the stratigraphic occurrence of the autochthonous (*in situ*) system in the middle zone is obviously vertically stratified (Wang et al., 2022). From the lower layer to the top, there is a south-dipping thrust

10.3389/feart.2023.1057936

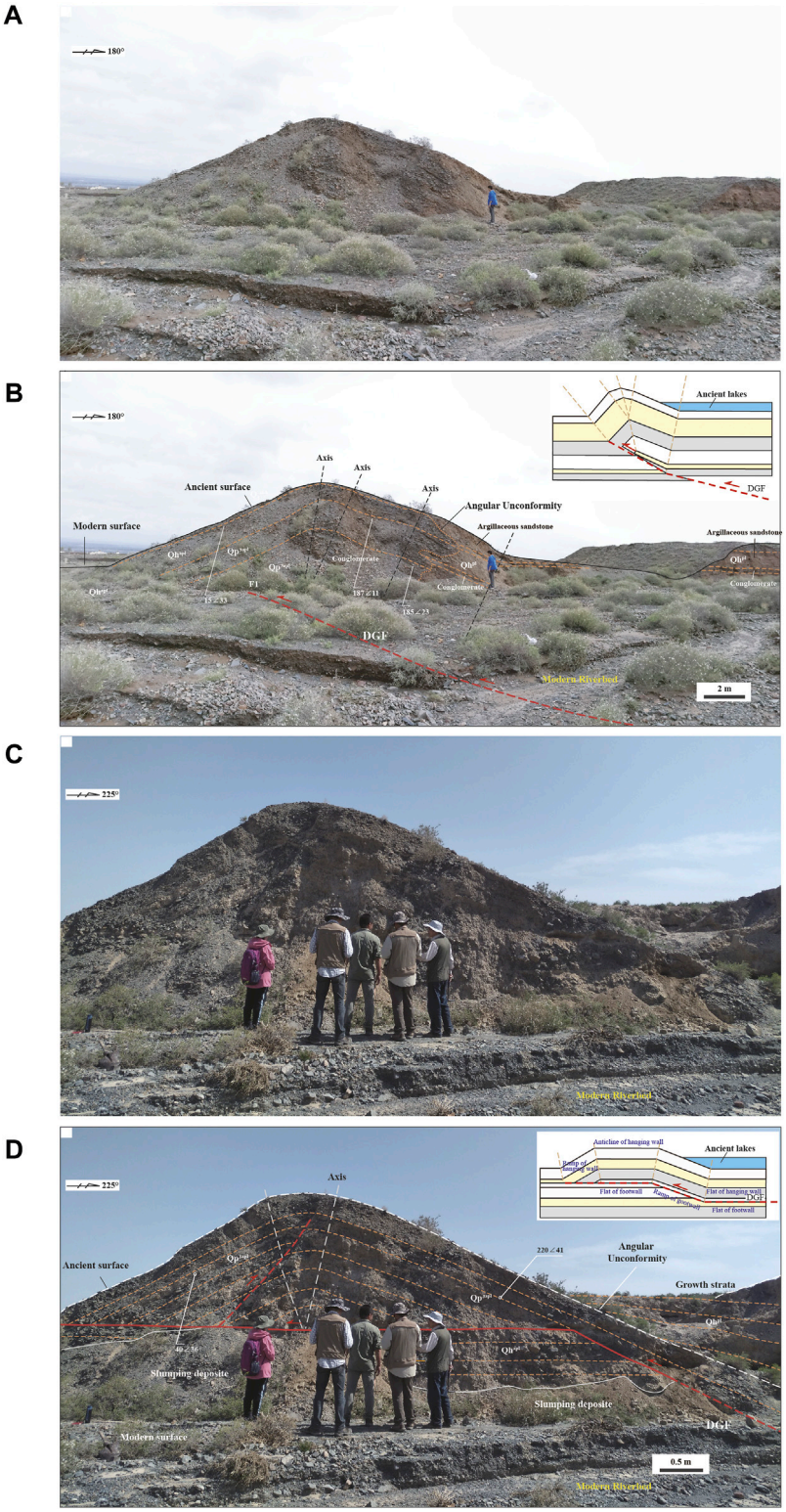

FIGURE 5
ross-sectional view of the Dagengzi anticline belt. The bulge-shaped belts in the surface indicate fault-propagation folding of the Holocene surface (Qh) and blind thrust along the Dagengzi Fault (DGF). The upper right corner shows a structural model for the fault-propagation fold **(A,B)**. Another cross-sectional view of the Dagengzi anticline belt. The bulge indicates fault-bend folding of the Holocene surface (Q_4) and thrusting ramp and flat of the DGF. The upper right corner shows a model for the fault-bend fold **(C,D)**. Bedding is expressed as the dipping direction and dip angle. Qp^{3apl}—alluvial–pluvial deposits of the Upper Pleistocene; Qh^{apl}—Holocene alluvial–pluvial deposits; Qh^{pl}—Holocene diluvial deposits. See location in Figure 3.

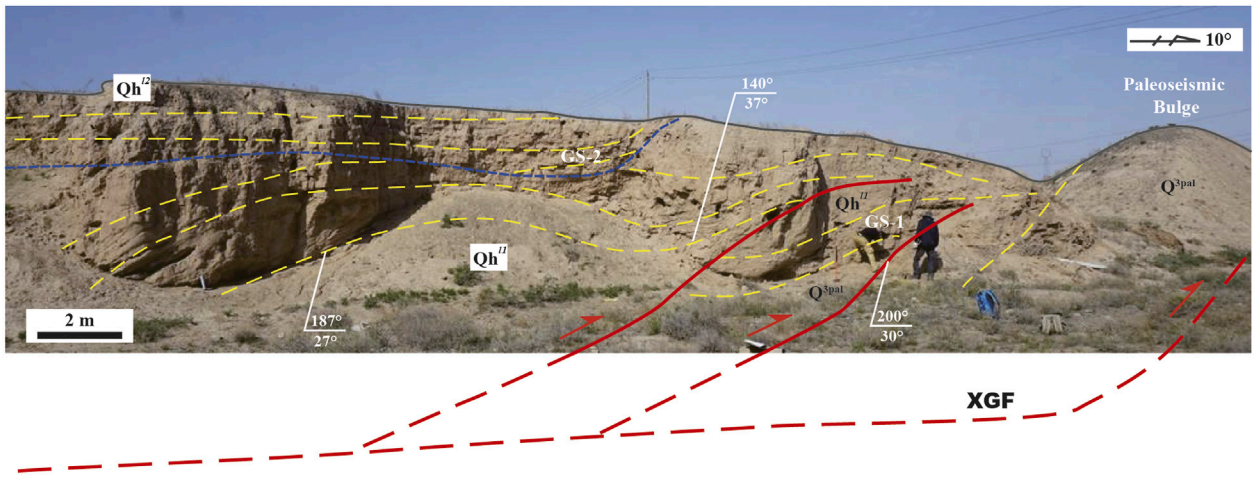

FIGURE 6
ross-sectional view of the Dagengzi Fault (DGF), showing imbricated thrusting along the blind DGF and folding of multi-stage growth strata. GS-1 and GS-2, two-stage growth strata. Qp^{3apl}, alluvial–pluvial deposits of the Upper Pleistocene. Qh^{I1} and Qh^{I2}, lower and upper layers of the Holocene lacustrine sediments. See location in Figure 3.

duplex developed in the Silurian strata, north-dipping overthrusts and fault-related folds formed in the Carboniferous and Permian strata, and gently folded Early Cretaceous basin sediments (Chen et al., 2019b; Wang et al., 2022). A series of klippes developed in the middle zone, including the Early Paleozoic granite intrusions exposed in the Jinyaosi and Panjiawan areas, the Silurian strata fragments scattered in the Early Cretaceous basin, and the remnant Carboniferous, Permian, Triassic, and Jurassic strata (Figure 2). The Neogene overlies the Cretaceous and scattered pre-Cretaceous klippes in the middle zone, with unconformity contact.

Our field investigation revealed that the Silurian flysch formation in the Yumu Shan is surrounded by thrust faults (i.e., the SYMF in the south and NYMF in the north), forming a klippe structure in the YMTS (Figures 2, 4). The SYMF is a northeast-dipping thrust fault exposed in the southern margin of the Yumu Shan (Figures 2, 3). It strikes ~120°–140° and dips ~30°–50° to the south. The NYMF is a thrust fault developed on the northern front of the Yumu Shan (Figures 2, 3). It strikes ~110° and dips ~35° to the north. The SYMF juxtaposes the Lower-Middle Silurian flysch over the Lower Cretaceous red beds and is unconformably covered by Quaternary strata (Figures 4A, D). Along the south-dipping NYMF, the Silurian strata are thrusted over strongly folded Devonian conglomerates and Lower Cretaceous red beds, and they are unconformably covered by folded Neogene strata (Figure 4B). In the northern slope of the Yumu Shan, the Carboniferous strata are surrounded by thrust faults (Figure 4C) and constitute a structural window with the Devonian in hanging walls (Figure 3). To the north, we did not observe additional klippes. Therefore, we conclude that the Yumu Shan is the frontal zone of the YMTS and that the NYMF is its northern front (Figures 2, 3).

The Hexi corridor active fault system

The Hexi Corridor active fault system is the reactivation and northward expansion of the YMTS since the Miocene (Chen et al., 2019b). In the Yumu Shan and adjacent area, the Hexi Corridor active fault system consists of a series of blind thrusts such as the Dagengzi Fault (DGF; also named the Gaotai Station Fault; Chen et al., 2006) and the Xiaogenzi Fault (XGF) in the northern front of the Yumu Shan, the westward extending strike–slipping of the SYMF (Figure 2), and the extensional normal faulting along the Zhangye Fault near Zhangye City.

There are two to three or four rows of nearly parallel bulge belts along the northern front of the Yumu Shan, south of the ruins of Camel City, once the capital city of the ancient Beiliang Kingdom (AD 397–439) and an important town in the Tang Dynasty (AD 618–907). The bulge belts are exposed as curved linear structures in the late Pleistocene (Q_p) alluvial fan, with a span of ca. 6 km and northeastward protruding. Google Earth image interpretation and structural geological mapping in the field revealed active blind and locally exposed thrust faulting along these belts. There are three to four south-dipping thrust faults, particularly the DGF, XGF, and their branch faults. The XGF splits into two or three WNW-striking thrusts in the Wutongquan area to the west, and it merges into the NW-striking Gaotai Station Fault (another name of the XGF) to the east (Figure 3).

The bulges are mainly composed of upper Pleistocene (Q_p^{apl}) and Holocene (Q_h^{apl}) deluvial–diluvium deposits (Figures 5A,B). These are mainly composed of sand and gravel layers with sandstone, with bedding and an inconspicuous layered structure. The bulges in the eastern segments, with heights of 1–5 m in general and ca. 8 m locally, are obviously of greater height than those in the western segments. The existence of tectonic relief (Chen et al., 2022b) between the bulges and the Holocene slope surface implies the overthrust of the bulges onto the slope. The hinterland of the thrust-related bulge belts is dominated by widely exposed Holocene lacustrine sediments (Figure 3).

Detailed structural analyses revealed that the geomorphic bulges are developed on hanging walls of blind thrusts, such as the Dagengzi and Xiaogengzi thrust faults, forming thrust-related anticlines (Figure 5). The bulges are characterized by asymmetric geometry, with steep limbs (dip angle of ca. 33°) in the north and relatively gentle limbs in the south

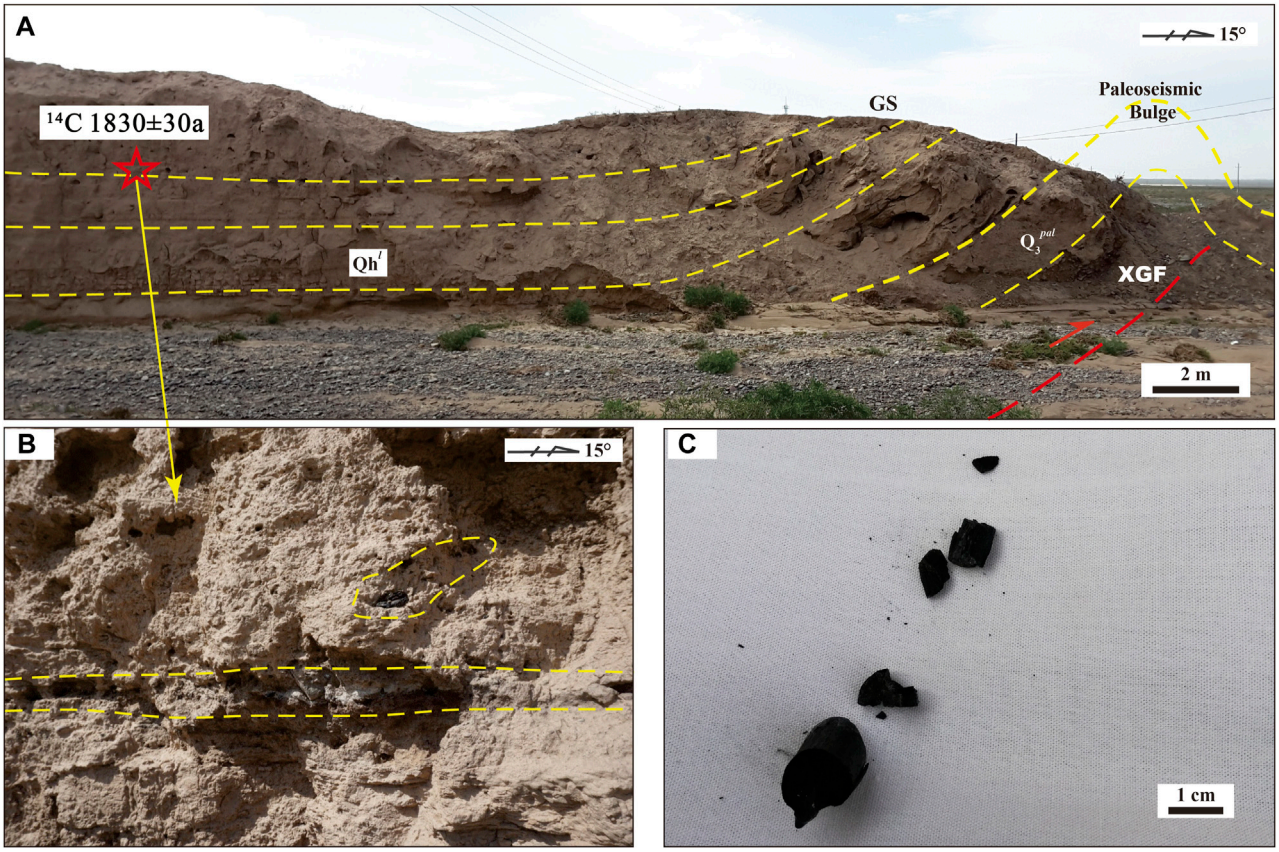

FIGURE 7
Structural analysis of the Dagengzi Fault (DGF). **(A)** Cross-sectional view of the blind DGF, showing the growth strata (GS), broken anticline, and sample locality of the plant charcoal. Qh^{l} —Holocene lacustrine sediments. **(B)** Occurrence of the plant charcoal layer in the Holocene lacustrine argillaceous siltstone formation. **(C)** Charcoal sample in detail. See location in Figure 3.

(dips of ca. 23°–11°), indicating the south-dipping obduction of the DGF. At the rear edge (i.e., the south side of the arc-shaped anticline belt), an ancient lake formed with Holocene lacustrine deposits of argillaceous sandstone, with a thickness of several meters to tens of meters (Q_h^{pl}; Figure 5). An angular unconformity and relatively tilted lacustrine sediments can be found between lacustrine deposits and folded bulges (Figures 5A, B), which may imply lateral current scouring on the bank of the ancient lake.

In some cases, the south-dipping DGF is exposed at the surface (Figures 5C, D), indicating progressive thrusting along the fault. For example, deformation patterns, such as the fault-bend fold shown in Figures 5C, D, could be the progressive development of the fault-propagation fold in Figures 5A, B. In this case, the Holocene lacustrine growth strata sequence formed in the rear edge of the bulge, recording progressive movement along the DGF, and the rotation of the rear limb of the anticline in the south (Figures 5C, D).

Multi-phase deformation recorded in lacustrine sediments

A series of thrust faults can be seen along the bulge belts and the inner sedimentary basin in the south. The faults are south-dipping at a medium-low angle, with the formation of a strong schistosity fault gouge along low-dipping areas locally. The faults typically have ramp-flat geometry. The fault-flat surface is distributed along different lithologic interfaces. The fault ramps upward across the bedding, and piggyback folds develop on the fault ramp plane, with the hanging wall fault ramps exposed. S-shaped folds can be seen in the Holocene lacustrine deposits on the hanging walls of the faults.

The lacustrine deposits constrained by the thrust-related anticline belts record multi-phase compressional deformation, including overstep-propagated imbricate thrusts. The most significant record is a series of growth strata and folded beddings (Qh^{l1}) in the hanging wall of the thrusting DGF, which is covered by horizontal bedding of the youngest stratum (Qh^{l2}) (Figure 6). First-phase thrusting along the DGF and thrust-related folding are recorded by the growth strata GS-1 (Qh^{l1}), with a thickness of ca. 60 cm, implying the initiation of the DGF and the formation of the anticline bulge in the early Holocene. Growth strata GS-2 (Qh^{l2}), with a thickness of ca. 0.5~2.0 m, overlie the S-shaped folds of GS-1, which are composed of the observed Holocene lacustrine sedimentary rocks, implying the formation of the GS-2 during the second stage of folding (Figure 6).

TABLE 1 Radiocarbon analysis of charcoal in lacustrine deposits. The sample was collected from the Camel City site (see Figure 7 for location).

Field sample number	Laboratory sample number	Conventional age† (yr B.P.)	Calibrated age‡ (Cal B.P.)	Calibrated calendar age‡ (B.C./A.D.)	Description
ZG20180913-2(7A)	Beta-507474	1810 ± 30	1830 ± 30	A.D. 117–252	Charcoal in lacustrine deposits

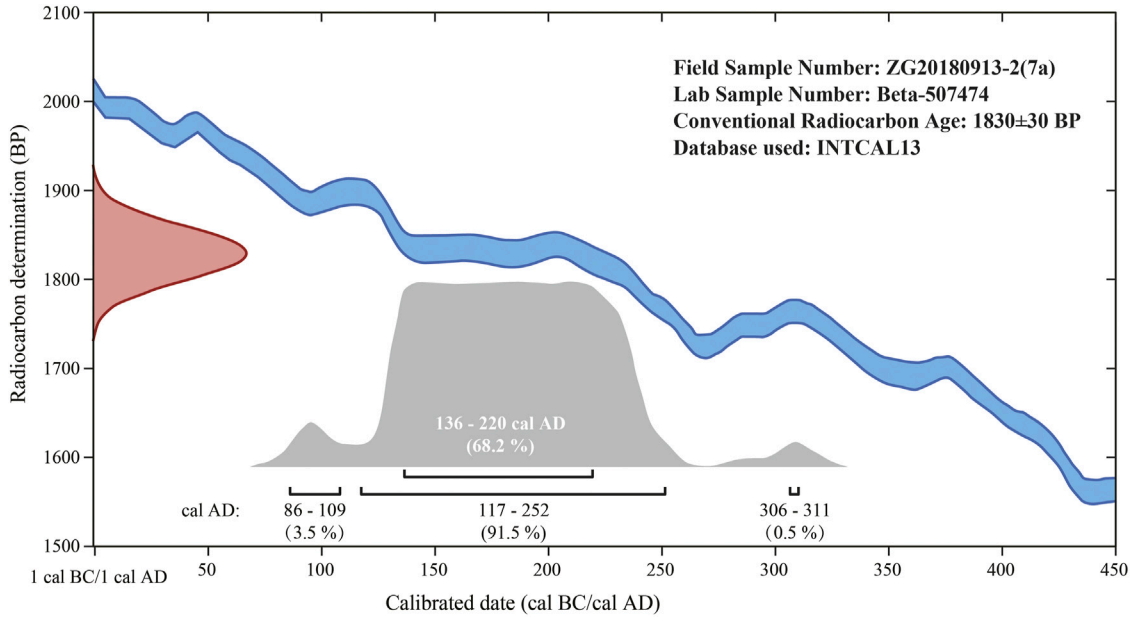

FIGURE 8
Calibrated ^{14}C ages for the charcoal sample from lacustrine deposits. Gray areas represent confidence probabilities, and high values represent high confidence levels. Each confidence interval corresponds to relative confidence probability (in parentheses).

Radiocarbon dating

Sampling and method

In this study, we adopted radiocarbon (^{14}C) dating of plant charcoal to determine the depositional age of the thrust-related lacustrine layer. We collected plant charcoal sample ZG20180913-2(7A) from the Holocene lacustrine deposits for ^{14}C dating (Figure 7). The sample is located in one layer of the growth strata sequence in the hinterland of the south-dipping DGF south of Camel City. Plant carbon debris (i.e., charcoals and burnt ashes) had been observed in the lacustrine layers, indicating that human activities or natural fires occurred there during the deposition stage of the lacustrine sedimentary materials. The ages of plant charcoals should be some records related to the thrusting along the DGF.

The charcoal sample was analyzed at Beta Analytic Inc. in the United States (lab test number Beta-507474) for ^{14}C AMS dating. Radiocarbon age was measured by accelerator mass spectrometer (AMS) and was referenced to the year A.D. 1950. The analytical uncertainty was reported at 2σ. Dendrochronologically calibrated calendar age, by Method A from CALIB Radiocarbon Calibration Version 7.0, was adopted (Stuiver and Reimer, 1993).

Measurement and result

Radiocarbon dating yielded an age in the range of 1830 ± 30 years Cal BP (Table 1; Figure 8). The $\delta^{13}C$ value of the sample was measured using an isotope ratio mass spectrometer (IRMS) at −23.9‰. This ratio was later used in the calculation of the radiocarbon age and error to correct for isotopic fractionation. The result reported the values of the sample measurement from the accelerator mass spectrometer (AMS), which were percent of modern carbon of 79.63 ± 0.30% pMC, fraction of modern carbon δ^{14} of −203.73‰ ± 2.97‰, and fraction of carbon δ^{14} of −210.25‰ ± 2.97‰ (1950: 2,018.00). The conventional age of the sample is 1810 ± 30 BP, whereas its calibrated age by BetaCal3.21 correction (isotopic fractionation $\delta^{13}C$ ratio, i.e., stable isotope ratios $^{12}C/^{13}C$) is 1830 ± 30 BP (in the Eastern Han Dynasty, using 1950 AD as 0 BP, i.e., all ^{14}C ages move back in time from 1950).

We used the high-probability density (HPD) range method (Bronk, 2009) to calibrate the calendar year for the sample. In other words, the INTCAL13 data sets (applicable to the northern hemisphere) were used to calibrate the conventional radiocarbon age (Reimer et al., 2013), and the relative confidence probabilities of 95.4% and 68.2% in all confidence intervals were statistical. Therefore, more accurate calendar ages were calculated as 117–252 cal. AD (91.5%), 86–109 cal. AD (3.5%), and

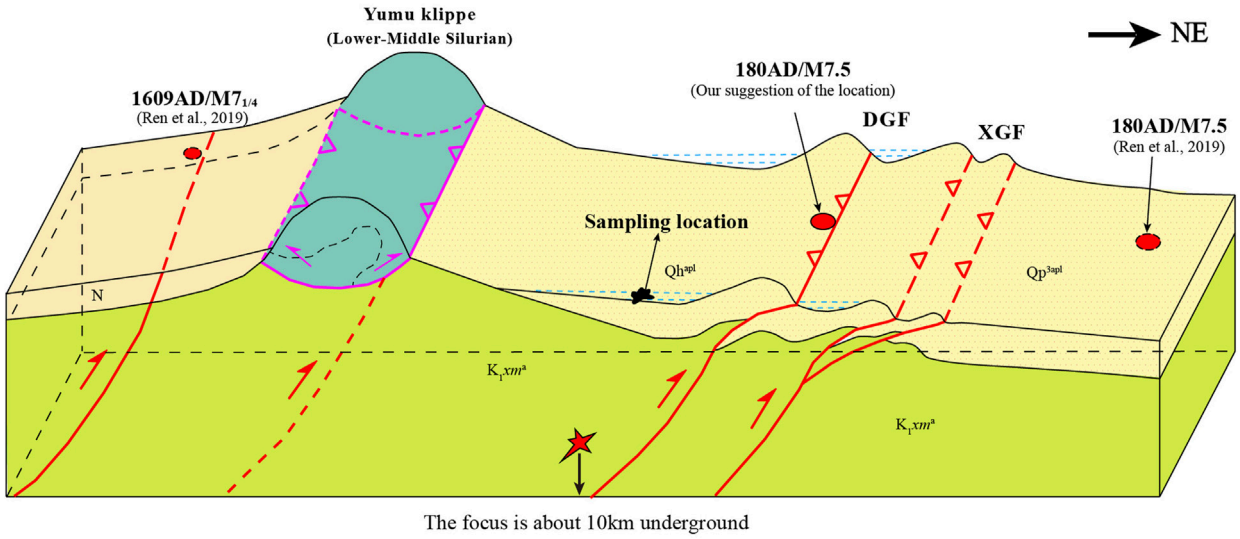

FIGURE 9
Structural model for the formation of the Dagengzi and Xiaogengzi faults and the 180AD/Ms7.5 Biaoshi earthquake, showing the northward expanding of the thrust faulting and growth of the plateau. DGF, Dagengzi Fault; XGF, Xiaogengzi Fault. Qp^{3apl}, alluvial–pluvial deposits of Upper Pleistocene; Qh^{apl}, Holocene alluvial–pluvial deposits.

306–311 cal. AD (0.5%) (Figure 8; the cal. AD is the calendar year, and the confidence probability is in parentheses).

To obtain an accurate radiocarbon date for the sample, we considered the "old wood effect" possibility and the mixing of younger materials, and we adopted the calendar age of the sample as A.D. 136–220 or A.D. 178 ± 42 (68.2%) in this study.

Discussion

Tectonic evolution in the northern margin of the Tibetan Plateau

The Qilian Shan in the northern Tibetan Plateau is considered an Early Paleozoic orogen and a reactivated fold-and-thrust belt in the Cenozoic (Yin and Harrison, 2000; Xiao et al., 2009; Chen et al., 2010; Yin, 2010; Li et al., 2018; Zuza et al., 2018; Li et al., 2021; Wu et al., 2021; Gao et al., 2022). Previous studies have revealed that the Qilian Shan fold-and-thrust belt is mainly a far-field response to the Indo-Asian continental collision in the Cenozoic (Tapponnier et al., 1990; Yin and Harrison, 2000; Hetzel et al., 2004; Zhang et al., 2004; Yin, 2006; Yin, 2010; Wang et al., 2014; Zhang et al., 2017; Yu et al., 2019; Zuza et al., 2019; Cheng et al., 2021). However, pre-Cenozoic tectonic events have played important roles in the uplift and lateral expanding of the Tibetan Plateau (Chen et al., 2019b; Li et al., 2021; Wang et al., 2022). In this work, we focused on the Mesozoic and Cenozoic tectonic evolution of the Yumu Shan, a junction between the northern Tibetan Plateau and the Hexi Corridor. The formation of the YMTS in the earlier Early Cretaceous is emphasized for its important role in shaping the embryonic form in the northern Tibetan Plateau. In the later Early to Late Cretaceous, right-lateral strike–slip and normal faulting extensively developed in the northern margin of the Tibetan Plateau (Vincent and Allen, 1999; Chen et al., 2003; Li, 2003; Chen et al., 2019b; Wang et al., 2022), which modified the study area significantly.

The tectonic evolution of the Yumu Shan played a critical role in the growth of the NE Tibetan Plateau, yet the uplift time of the Yumu Shan is still hotly debated. A thermal simulation study of bedrock AFT by Zheng et al. (2017) shows that the Yumu Shan was uplifted at approximately 4 Ma in the early Pliocene, which accords with magnetostratigraphic results (Liu et al., 2011), apatite fission track thermochronology dating (Wang et al., 2018), and research on the total structural relief and rates of rock uplift and denudation (Palumbo et al., 2009). Hu et al. (2022) suggest that the main range of the Yumu Shan was uplifted since ~3 Ma by the earlier thrust–fold system. Fang et al. (2012) suggest that the Yumu Shan began to uplift rapidly at approximately 9.8–9.6 Ma at the latest, rather than the previously thought much later rise of c. 1 Ma (Tapponnier et al., 1990; 2001; Metivier et al., 1998; Meyer et al., 1998). Chen et al. (2022) argue that rapid uplift of the Yumu Shan occurred at approximately 15–10 Ma and further developed at 10–5.1 Ma and 5.1–3.6 Ma. In the Jiuquan Basin, the angular unconformity in the Laojunmiao area indicates that the NE Tibetan Plateau underwent a powerful deformation and rapid uplift between ~0.9 and 0.8 Ma (Zhao et al., 2001; Liu et al., 2010). Our field investigation in this study revealed mainly blind and active thrusts in the north margin of the Yumu Shan, which may be responsible for the late Quaternary uplift in this area.

Active tectonics are widely developed along the Wutongquan, Camel City, and Xiaogengzi areas in the northern piedmont of the Yumu Shan. The DGF and XGF are the two most important active faults north to the Yumu Shan klippe, playing an important role in the northward expansion of the Tibetan Plateau. Previous research has detected two- to five-stage seismic activities along the DGF in the late Quaternary (Chen et al., 2006; Chen et al., 2008; Ren

et al., 2019). Our detailed geologic mapping in the field revealed south-dipping overthrust and thrust-related anticlines along the DGF (Figures 5A–D). Structural analyses of arcuate bulge belts, comprising these anticlines, led us to construct the tectonic model, as shown in Figure 9, and to suggest the progressive northeastward development of active thrusts in the Hexi Corridor. The existence of growth strata indicates anticline-related thrusting in the Holocene. Since the most northern location of the XGF is among the blind thrusts in the northern slope of the Yumu Shan, we suggest the XGF as the north boundary thrust (NBT) defining the northern boundary of the Tibetan Plateau in this region.

Historical earthquakes and formation of geomorphic bulge belts

The Yumu Shan region has undergone many periods of historical earthquakes. The most recent paleo-earthquake, the Hongyazi earthquake (1609 AD/M $7_{1/4}$), occurred in the middle zone of the YMTS, southwest of the Yumu Shan klippe. An earlier paleo-earthquake, the Biaoshi earthquake (180 AD/M7.5), occurred at the northern front of the Yumu Shan near Camel City (Figure 2; Tapponnier et al., 1990; Yang et al., 2018a; Ren et al., 2019). Historical documents show that the year A.D. 180 was in the third Guanghe Era of the reign of Emperor Ling of the Eastern Han Dynasty. In the autumn of this year, temples and folk buildings in Biaoshi City were destroyed by the earthquake with water eruption. In other words, there was a major flood event, followed by the great earthquake. Afterward, Camel City was chosen to be rebuilt as the new city (Figure 2). More recently, east to the Yumu Shan, a 1954/M7.3 earthquake occurred near Minle County in the Hexi corridor (Ren et al., 2019). Most recently, the China Seismic Network reported an Ms5.0 earthquake, occurring at 20:48 on 16 September 2019, in Ganzhou District, Zhangye, Gansu Province, with a focal depth of 11 km and an epicenter located at 38.60 N and 100.35 E. The location is between the 180 AD/M7.5 Biaoshi and 1954/M7.3 Minle earthquakes.

A previous study suggested that the Fodongmiao–Hongyazi segment of the NQLF may accommodate ca. 15%–20% of the total crustal shortening across the Qilian Shan since the late Pleistocene (Yang et al., 2018b), implying the reactivation of the NQLF during the Quaternary. According to the spatiotemporal distribution of major paleo-earthquakes, active thrust faulting is out of sequence surrounding the Yumu Shan klippe, and the seismogenic faults could be some blind thrusts around the Yumu Shan but not the NQLF far to the south. The radiocarbon age of A.D. 178 ± 42 obtained for the charcoal sample in this study is close to the time of the 180 AD/M 7.5 Biaoshi earthquake (Yang et al., 2018a). The similarity between the paleo-seismic event and the lacustrine sedimentary age implies that historical earthquakes, especially the Biaoshi earthquake, might have led to the formation of geomorphic bulges, resulting in lacustrine deposition in their hinterlands. Our detailed structural analyses provide new evidence for the tectonic origin of the geomorphic bulges. We suggest that the formation of these arcuate belts of bulges might have resulted from the active blind thrust faulting and fault-related folding in the region. The bulge belts are not artificial dams. The existence of multi-stage growth strata and imbricated thrusts in lacustrine layers indicates a sequence of historical earthquakes along the DGF (Figure 6). Furthermore, ancient lakes in the hinterland of the bulge belts might be thrust-related due to the blocking of the floods by the high relief barrier of the bulges (Figure 9). Therefore, we suggest that the XGF might be the seismogenic fault for the 180 AD/M 7.5 Biaoshi earthquake, although its location as suggested by Ren et al. (2019) is further north of Camel City (Figure 2).

Conclusion

Based on detailed field investigations, structural mapping and analysis, and radiocarbon dating of lacustrine sediments associated with active blind thrusts in northern Yumu Shan, the junction region between the Tibetan Plateau and Hexi Corridor, we reached the following conclusions.

(1) The active tectonics are distributed along the Wutongquan–Camel City–XiaoGengzi area in the mountain front north of the Yumu Shan, northern Tibetan Plateau. They are dominated by arcuate anticline belts that protrude toward the NE. We interpret these active anticlines as thrust-related folds resulting from northeastward blind thrusting in the northern piedmont of the Yumu Shan, which caused the northeastward growth of the Tibetan Plateau. Among these active thrusts, the Xiaogengzi Fault is the most northeastern (i.e., the North Boundary Thrust) and defines the northeastern margin of the Tibetan Plateau in the Yumu Shan region.
(2) Owing to the water-holding capacity of the arcuate anticline belts, lacustrine sediments were deposited subsequently along their hinterlands. ^{14}C dating of a plant charcoal sample from one of the lacustrine sedimentary layers yielded an age of AD 178 ± 42, indicating the formation of the arcuate anticline belts at this time. It is close to the AD180 Ms.7.5 Biaoshi Earthquake in the Eastern Han Dynasty in both age and location. Therefore, we suggest that these active tectonics, such as the blind thrusts and related anticline belts, were caused by paleo-earthquakes such as the Biaoshi earthquake. Our study implies that paleo-earthquakes were responsible for the northward growth of the Tibetan Plateau.

Data availability statement

The original contributions presented in the study are included in the article/Supplementary Material; further inquiries can be directed to the corresponding author.

Author contributions

YW: conceptualization, methodology, field mapping, visualization, and writing—original draft, review, and editing. XC: funding acquisition, conceptualization, methodology, supervision, field mapping, visualization, and writing–review and editing. CH: field mapping and writing—review. YX: methodology and data curation. ZS: funding acquisition and field mapping. J'eH: field

mapping and methodology. BL, YZ, WD, SX, and LH: field mapping and visualization.

Funding

This study was support by the China Geological Survey (Nos. DD20230008, DD20190011, and DD20160083), the National Key Research and Development Program of China (the DREAMDeep Resource Exploration and Advanced Mining; No. 2018YFC0603701), and the Cooperative Project of Chinese Academy of Geological Sciences (No. P22065).

Acknowledgments

The authors would like to thank Zengzhen Wang, Yongchao Wang, Yaoyao Zhang, Jianjie Shi, Guodian Bai, Kaiwen Li, Haohao Shao, Huixin Miao, and Jie Li for their help in the fieldwork.

Conflict of interest

Author YX was employed by Sinopec Shengli Oilfield Company.

The remaining authors declare that the research was conducted in the absence of any commercial or financial relationships that could be construed as a potential conflict of interest.

The reviewer DL declared a shared affiliation with the author JH to the handling editor at the time of review.

Publisher's note

References

BGGP (1971). *Bureau of geology of Gansu Province (BGGP, first regional geological survey), geologic map of sunan region, scale 1:200,000*. Beijing, China: Ministry of Geology of China.

BGGP (1973). *Bureau of geology of Gansu Province (BGGP, first regional geological survey), geologic map of Zhangye region, scale 1:200,000*. Beijing, China: Ministry of Geology of China.

Bronk, R. C. (2009). Bayesian analysis of radiocarbon dates. *Radiocarbon* 51 (1), 337–360. doi:10.1017/s0033822200033865

Chen, B., Wang, C., Cui, L., and Liu, J. (2008). Developing model of thrust fault system in Western part of northern Qilian Mountains margin – Hexi Corridor basin during late Quaternary. *Earth Sci. Front.* 15 (6), 260–277.

Chen, B., Wang, C., Liu, J., Liu, J., and Zhang, Y. (2006). The activity of the xinminbao fault from the late Pleistocene to Holocene. *Acta Geol. sin-engl.* 27 (6), 515–524.

Chen, G., Zheng, W., Wang, X., Zhang, P., Xiong, J., Yu, J., et al. (2017). Present kinematics characteristics of the northern Yumushan active fault and its response to the northeastward growth of the Tibetan Plateau. *Seismol. Geol.* 39 (5), 871–888.

Chen, L. H., Wang, Y. D., He, P. J., Song, C. S., Meng, Q. Q., Feng, W., et al. (2022). Mesozoic-Cenozoic multistage tectonic deformation of the Qilian Shan constrained by detrital apatite fission track and zircon U–Pb geochronology in the Yumu Shan area. *Tectonophysics* 822 (5), 229151. doi:10.1016/j.tecto.2021.229151

Chen, P., Shi, W., Hu, J., Yan, B., and Lu, H. (2021). Identification of the seismogenic fault of the 1654 M 8.0 tianshui earthquake, northeastern Tibetan plateau. *Seismol. Res. Lett.* 92, 2943–2951. doi:10.1785/0220200256

Chen, X. H., Chen, Z. L., Shao, Z. G., Zhang, Y. P., Li, B., Ding, W. C., et al. (2022b). Theory of tectonic relief analysis and its application in geoscience. *Acta Geol. Sin.* 96 (1), 284–296.

Chen, X. H., Dang, Y., Yin, A., Wang, L., Jiang, W., Jiang, R., et al. (2010). *Basin-mountain coupling and tectonic evolution of Qaidam Basin and its adjacent orogenic belts*. Beijing: Geological Publishing House, 1–365.

Chen, X. H., Dong, S. W., Shi, W., Ding, W. C., Zhang, Y. P., Li, B., et al. (2022a). Construction of the continental asia in phanerozoic: A review. *Acta Geol. sin-engl.* 96 (1), 26–51. doi:10.1111/1755-6724.14867

Chen, X. H., Shao, Z. G., Xiong, X. S., Gao, R., Liu, X. J., Wang, C. F., et al. (2019a). Fault system, deep structure and tectonic evolution of the Qilian Orogenic Belt, Northwest China. *Geol. China* 46 (5), 995–1020.

Chen, X. H., Shao, Z. G., Xiong, X. S., Gao, R., Xu, S. L., Zhang, Y. P., et al. (2019b). Early cretaceous overthrusting of yumushan mountain and hydrocarbon prospect on the northern margin of the qilian orogenic belt. *Acta Geosci. Sin.* 40 (3), 377–392.

Chen, X. H., Yin, A., Gehrels, G. E., Cowgill, E. S., Grove, M., Harrison, T. M., et al. (2003). Two phases of Mesozoic north-south extension in the eastern Altyn Tagh range, northern Tibetan Plateau. *Tectonics* 22 (5), 1053. doi:10.1029/2001tc001336

Cheng, F., Zuza, A. V., Haproff, P. J., Wu, C., Neudorf, C., Chang, H., et al. (2021). Accommodation of India-Asia convergence via strike–slip faulting and block rotation in the Qilian Shan fold-thrust belt, northern margin of the Tibetan Plateau. *J. Geol. Soc.* 178, jgs2020–207. doi:10.1144/jgs2020-207

Clark, M. K., and Royden, L. H. (2000). Topographic ooze: Building the eastern margin of Tibet by lower crustal flow. *Geology* 28, 703–706. doi:10.1130/0091-7613(2000)028<0703:tobtem>2.3.co;2

Coward, M. P., Kidd, W., Yun, P., Shackleton, R. M., and Hu, Z. (1988). The structure of the 1985 Tibet geotraverse, Lhasa to Golmud. *Philos. Trans. R. Soc. Lond. A. Math. Phys.* 327 (1594), 307–333.

Fang, X., Liu, D., Song, C., Dai, S., and Meng, Q. (2012). Oligocene slow and MioceneQuaternary rapid deformation and uplift of the Yumu Shan and North Qilian Shan:evidence from high-resolution magnetostratigraphy and tectonosedimentology. *Geol. Soc. Lond., Spec. Publ.* 373 (1), 149–171. doi:10.1144/sp373.5

Gao, R., Li, T., and Wu, G. (1998). Lithospheric evolution and geodynamic process of the Qinghai-Tibet Plateau: An inspiration from the Yadong-Golmud-Ejin geoscience transect. *Geol. Rev.* 44 (4), 389–395.

Gao, R., Qi, R., Huang, X. F., Chen, X. H., Xiong, X. S., Guo, X. Y., et al. (2022). Disclosure of high-resolution crustal structure beneath the central region of Qilian Shan, northeastern Tibetan Plateau. *Chin. J. Geophys.* 65 (8), 2857–2871.

George, A. D., Marshallsea, S. J., Wyrwoll, K. H., Jie, C., and Yanchou, L. (2001). Miocene cooling in the northern Qilian Shan, northeastern margin of the Tibetan Plateau, revealed by apatite fission-track and vitrinite-reflectance analysis. *Geology* 29, 939–942. doi:10.1130/0091-7613(2001)029<0939:MCITNQ>2.0.CO;2

Harris, N. B. W., Ronghua, X., Lewis, C. L., and Chengwei, J. (1988). Plutonic rocks of the 1985 Tibet geotraverse, Lhasa to Golmud. *Philos. Trans. R. Soc. Lond. A. Math. Phys.* 327 (1594), 145–168.

Hetzel, R., Tao, M., Stokes, S., Niedermann, S., Ivy-Ochs, S., Gao, B., et al. (2004). Late Pleistocene/Holocene slip rate of the Zhangye thrust (Qilian Shan, China) and implications for the active growth of the northeastern Tibetan Plateau. *Tectonics* 23 (6), TC6006.1–TC6006.17. doi:10.1029/2004tc001653

Hu, X., Wu, J., Wen, Z., Zhang, J., Zhao, Q., and Pan, B. (2022). Fluvial evolution in a growing thrust-fold range of the Yumu Shan, NE Tibetan Plateau. *Earth Planet. Sci. Lett.* 594, 117704. doi:10.1016/j.epsl.2022.117704

Huntington, K. W., Blythe, A. E., and Hodges, K. V. (2006). Climate change and late Pliocene acceleration of erosion in the Himalaya. *Earth Planet. Sci. Lett.* 252 (1-2), 107–118. doi:10.1016/j.epsl.2006.09.031

Kidd, W. S., and Molnar, P. (1988). Quaternary and active faulting observed on the 1985 academia sinica-royal society geotraverse of Tibet. *Philos. Trans. R. Soc. Lond. A. Math. Phys.* 327 (1594), 337–363.

Li, B., Chen, X. H., Zuza, A. V., Hu, D., Ding, W., Huang, P., et al. (2019). Cenozoic cooling history of the North Qilian Shan, northern Tibetan Plateau, and the initiation of the Haiyuan fault: Constraints from apatite- and zircon-fission track thermochronology. *Tectonophysics* 751, 109–124. doi:10.1016/j.tecto.2018.12.005

Li, B., Zuza, A. V., Chen, X. H., Hu, D. G., Shao, Z. G., Qi, B. S., et al. (2020). Cenozoic multi-phase deformation in the Qilian Shan and out-of-sequence development of the northern Tibetan Plateau. *Tectonophysics* 782-783, 228423. doi:10.1016/j.tecto.2020.228423

Li, B., Zuza, A. V., Chen, X. H., Wang, Z. Z., Shao, Z. G., Levy, D. A., et al. (2021). Pre-Cenozoic evolution of the northern Qilian Orogen from zircon geochronology: Framework for early growth of the northern Tibetan Plateau. *Palaeogeogr. Palaeoclimatol. Palaeoecol.* 562, 110091. doi:10.1016/j.palaeo.2020.110091

Li, F. Q. (2003). New evidence for the presence of the NS-trending extensional structures in northwestern China: An example from the Early Cretaceous half graben fault depressions in Jiuquan, Gansu. *Sediment. Geol. Tethyan Geol.* 23 (2), 35–42.

Li, S. Z., Zhao, S. J., Liu, X., Cao, H. H., Yu, S., Li, X. Y., et al. (2018). Closure of the proto-tethys Ocean and early paleozoic amalgamation of microcontinental blocks in east asia. *Earth-Sci. Rev.* 186, 37–75. doi:10.1016/j.earscirev.2017.01.011

Li, Y. L., Yang, J. C., Tan, L. H., and Duan, F. J. (1999). Impact of tectonics on alluvial landforms in the Hexi corridor, northwest China. *Geomorphology* 28, 299–308. doi:10.1016/s0169-555x(98)00114-7

Liu, D., Fang, X., Song, C., Dai, S., Zhang, T., Zhang, W., et al. (2010). Stratigraphic and paleomagnetic evidence of mid-Pleistocene rapid deformation and uplift of the NE Tibetan Plateau. *Tectonophysics* 486 (1–4), 108–119. doi:10.1016/j.tecto.2010.01.014

Liu, D., Yan, M., Fang, X., Li, H., Song, C., and Dai, S. (2011). Magnetostratigraphy of sediments from the Yumu Shan, Hexi corridor and its implications regarding the late cenozoic uplift of the NE Tibetan plateau. *Quat. Int.* 236 (1–2), 13–20. doi:10.1016/j.quaint.2010.12.007

Métivier, F., Gaudemer, Y., Tapponnier, P., and Meyer, B. (1998). Northeastward growth of the Tibet plateau deduced from balanced reconstruction of two depositional areas: The Qaidam and Hexi Corridor basins, China. *Tectonics* 17 (6), 823–842. doi:10.1029/98tc02764

Meyer, B., Tapponnier, P., Bourjot, L., Métivier, F., Gaudemer, Y., Peltzer, G., et al. (1998). Crustal thickening in Gansu-Qinghai, lithospheric mantle subduction, and oblique, strike–slip controlled growth of the Tibet plateau. *Geophys. J. Int.* 135 (1), 1–47. doi:10.1046/j.1365-246x.1998.00567.x

Molnar, P. (1988). Continental tectonics in the aftermath of plate tectonics. *Nature* 335, 131–137. doi:10.1038/335131a0

Palumbo, L., Hetzel, R., Tao, M., Li, X., and Guo, J. (2009). Deciphering the rate of mountain growth during topographic presteady state: An example from the NE margin of the Tibetan plateau. *Tectonics* 28 (4), 2455. doi:10.1029/2009tc002455

Reimer, P., Bard, E., Bayliss, A., Beck, J., Blackwell, P., Ramsey, C., et al. (2013). IntCal13 and Marine13 radiocarbon age calibration curves 0–50,000 Years cal BP. *Radiocarbon* 55 (4), 1869–1887. doi:10.2458/azu_js_rc.55.16947

Ren, J. J., Xu, X. W., Zhang, S. M., Ding, R., Liu, H. Y., Liang, O. B., et al. (2019). Late Quaternary slip rates and Holocene paleoearthquakes of the eastern Yumu Shan fault, northeast Tibet: Implications for kinematic mechanism and seismic hazard. *J. Asian Earth Sci.* 176, 42–56. doi:10.1016/j.jseaes.2019.02.006

Royden, L. H., Burchfiel, B. C., King, R. W., Wang, E., Chen, Z., Shen, F., et al. (1997). Surface deformation and lower crustal flow in eastern Tibet. *Science* 276, 788–790. doi:10.1126/science.276.5313.788

Royden, L. H., Clark, B., and van der Hilst, R. D. (2008). The geological evolution of the Tibetan Plateau. *Science* 321 (5892), 1054–1058. doi:10.1126/science.1155371

Song, S. G., Niu, Y. L., Su, L., Zhang, C., and Zhang, L. F. (2014). Continental orogenesis from ocean subduction, continent collision/subduction, to orogen collapse, and orogen recycling: The example of the North Qaidam UHPM belt, NW China. *Earth-Sci. Rev.* 129, 59–84. doi:10.1016/j.earscirev.2013.11.010

Stuiver, M., and Reimer, P. J. (1993). Extended ^{14}C data base and revised Calib 3.0 ^{14}C age calibration program. *Radiocarbon* 35, 215–230. doi:10.1017/s0033822200013904

Sukhija, B. S., Reddy, D. V., Kumar, D., and Nagabhushanam, P. (2006). Comment on "Interpreting the style of faulting and paleoseismicity associated with the 1897 Shillong, northeast India, earthquake" by C. P. Rajendran et al. *Tectonics* 25, 0278–7407. doi:10.1029/2005TC001893

Tapponnier, P., Meyer, B., Avouac, J. P., Peltzer, G., Gaudemer, Y., Guo, S., et al. (1990). Active thrusting and folding in the Qilian Shan, and decoupling between upper crust and mantle in northeastern Tibet. *Earth Planet. Sci. Lett.* 97 (3), 382–403. doi:10.1016/0012-821x(90)90053-z

Tapponnier, P., Peltzer, G., and Armijo, R. (1986). On the mechanics of the collision between India and Asia. *Spec. Publ. - Geol. Soc. Lond.* 19, 113–157. doi:10.1144/gsl.sp.1986.019.01.07

Tapponnier, P., Peltzer, G., Le Dain, A. Y., Armijo, R., and Cobbold, P. (1982). Propagating extrusion tectonics in asia: New insights from simple experiments with plasticine. *Geology* 10, 611–616. doi:10.1130/0091-7613(1982)10<611:petian>2.0.co;2

Tapponnier, P., Xu, Z., Roger, F., Meyer, B., Arnaud, N., Wittlinger, G., et al. (2001). Oblique stepwise rise and growth of the Tibet Plateau. *Science* 294 (5547), 1671–1677. doi:10.1126/science.105978

Vincent, S. J., and Allen, M. B. (1999). Evolution of the Minle and chaoshui basins, China: Implications for mesozoic strike–slip basin formation in central asia. *Bull. Geol. Soc. Am.* 111, 725–742. doi:10.1130/0016-7606(1999)111<0725:eotmac>2.3.co;2

Wang, C. S., Dai, J., Zhao, X., Li, Y., Graham, S., He, D., et al. (2014). Outward growth of the Tibetan plateau during the cenozoic: A review. *Tectonophysics* 621, 1–43. doi:10.1016/j.tecto.2014.01.036

Wang, Y., Chen, X. H., Nie, L. S., Ding, W. C., Wang, X. Q., Xu, S. L., et al. (2020). Late Paleozoic element migration and accumulation under intracontinental sinistral strike–slip faulting in the West Junggar Orogenic Belt, NW China. *Acta Geol. sin-engl.* 94 (6), 2012–2030. doi:10.1111/1755-6724.14608

Wang, Y., Chen, X. H., Zhang, Y. Y., Yin, Z., Zuza, A. V., Yin, A., et al. (2022). Superposition of cretaceous and cenozoic deformation in northern Tibet: A far-field response to the tectonic evolution of the tethyan orogenic system. *Geol. Soc. Am. Bull.* 134 (1-2), 501–525. doi:10.1130/b35944.1

Wang, Y., Zheng, D., Pang, J., Zhang, H., Wang, W., Yu, J., et al. (2018). Using slope-area and apatite fission track analysis to decipher the rock uplift pattern of the Yumu Shan: New insights into the growth of the NE Tibetan Plateau. *Geomorphology* 308, 118–128. doi:10.1016/j.geomorph.2018.02.006

Wu, C., Zuza, A. V., Yin, A., Chen, X. H., Haproff, P. J., Li, J., et al. (2021). Punctuated orogeny during the assembly of asia: Tectonostratigraphic evolution of the North China craton and the qilian Shan from the paleoproterozoic to early paleozoic. *Tectonics* 40 (4), 0278–7407. doi:10.1029/2020tc006503

Xiao, W. J., Windley, B. F., Yong, Y., Yan, Z., Yuan, C., Liu, C. Z., et al. (2009). Early paleozoic to devonian multiple-accretionary model for the qilian Shan, NW China. *J. Asian Earth Sci.* 35, 323–333. doi:10.1016/j.jseaes.2008.10.001

Yang, H. B., Yang, X. P., Huang, X. N., Li, A., Huang, W. L., and Zhang, L. (2018b). New constraints on slip rates of the Fodongmiao-Hongyazi fault in the Northern Qilian Shan, NE Tibet, from the ^{10}Be exposure dating of offset terraces. *J. Asian Earth Sci.* 151, 131–147. doi:10.1016/j.jseaes.2017.10.034

Yang, H. B., Yang, X. P., Zhang, H. P., Huang, X. N., Huang, W. L., and Zhang, N. (2018a). Active fold deformation and crustal shortening rates of the Qilian Shan foreland thrust belt, NE Tibet, since the Late Pleistocene. *Tectonophysics* 742-743, 84–100. doi:10.1016/j.tecto.2018.05.019

Yin, A. (2010). Cenozoic tectonic evolution of asia: A preliminary synthesis. *Tectonophysics* 488, 293–325. doi:10.1016/j.tecto.2009.06.002

Yin, A. (2006). Cenozoic tectonic evolution of the Himalayan orogen as constrained by along strike variation of structural geometry, exhumation history, and foreland sedimentation. *Earth Sci. Rev.* 76 (1–2), 1–131. doi:10.1016/j.earscirev.2005.05.004

Yin, A., Dang, Y. Q., Wang, L. C., Jiang, W. M., Zhou, S. P., Chen, X. H., et al. (2008a). Cenozoic tectonic evolution of Qaidam Basin and its surrounding regions (part 1): The southern Qilian Shan–Nan Shan thrust belt and northern Qaidam Basin. *Geol. Soc. Am. Bull.* 120 (7-8), 813–846. doi:10.1130/b26180.1

Yin, A., Dang, Y. Q., Zhang, M., Chen, X. H., and McRivette, M. W. (2008b). Cenozoic tectonic evolution of the Qaidam Basin and its surrounding regions (Part 3): Structural geology, sedimentation, and regional tectonic reconstruction. *Geol. Soc. Am. Bull.* 120 (7-8), 847–876. doi:10.1130/b26232.1

Yin, A., and Harrison, T. M. (2000). Geologic evolution of the himalayan-Tibetan orogen. *Annu. Rev. Earth Planet. Sci.* 28 (28), 211–280. doi:10.1146/annurev.earth.28.1.211

Yin, A., Rumelhart, P. E., Butler, R., Cowgill, E., Harrison, T. M., Foster, D. A., et al. (2002). Tectonic history of the Altyn Tagh fault system in northern Tibet inferred from Cenozoic sedimentation. *Geol. Soc. Am. Bull.* 114 (10), 1257–1295. doi:10.1130/0016-7606(2002)114<1257:thotat>2.0.co;2

Yu, J. X., Pang, J. Z., Wang, Y. Z., Zheng, D. W., Liu, C. C., Wang, W. T., et al. (2019). Mid-Miocene uplift of the northern Qilian Shan as a result of the northward growth of the northern Tibetan Plateau. *Geosphere* 15 (2), 423–432. doi:10.1130/ges01520.1

Yu, Z. Y., Yin, N., Wang, C. Y., Deng, M., and Lan, W. G. (2021). Active tectonics, paleoseismology and seismic hazards of the piedmont Xizhoushan fault zone in the Shanxi graben system, North China Block. *J. Asian Earth Sci.* 205, 104590. doi:10.1016/j.jseaes.2020.104590

Zhang, H. P., Zhang, P. Z., Prush, V., Zheng, D. W., Zheng, W. J., Wang, W. T., et al. (2017). Tectonic geomorphology of the Qilian Shan in the northeastern Tibetan Plateau: Insights into the plateau formation processes. *Tectonophysics* 706-707, 103–115. doi:10.1016/j.tecto.2017.04.016

Zhang, P. Z., Shen, Z. K., Wang, M., Gan, W. J., Bürgmann, R., Molnar, P., et al. (2004). Continuous deformation of the Tibetan Plateau from global positioning system data. *Geology* 32 (9), 809–812. doi:10.1130/g20554.1

Zhao, Z. J., Fang, X. M., Li, J. J., Pan, B. T., Yan, M. D., and Shi, Z. T. (2001). Paleomagnetic dating of the jiuquan gravel in the Hexi corridor: Implication on mid-pleistocene uplift of the Qinghai-Tibetan plateau. *Chin. Sci. Bull.* 46 (23), 2001–2005. doi:10.1007/bf02901916

Zheng, D., Wang, W., Wan, J., Yuan, D., Liu, C., Zheng, W., et al. (2017). Progressive northward growth of the northern qilian Shan–Hexi corridor (northeastern Tibet) during the cenozoic. *Lithosphere* 9 (3), 408–416. doi:10.1130/l587.1

Zheng, W. J., Zhang, P. Z., Ge, W. P., Molnar, P., Zhang, H. P., Yuan, D. Y., et al. (2013). Late quaternary slip rate of the South Heli Shan fault (northern Hexi corridor, NW China) and its implications for northeastward growth of the Tibetan plateau. *Tectonics* 32, 271–293. doi:10.1002/tect.20022

Zuza, A. V., Wu, C., Reith, R. C., Yin, A., Li, J. H., Zhang, J. Y., et al. (2018). Tectonic evolution of the Qilian Shan: An early Paleozoic orogen reactivated in the Cenozoic. *Geol. Soc. Am. Bull.* 130 (5-6), 881–925. doi:10.1130/b31721.1

Zuza, A. V., Wu, C., Wang, Z. Z., Levy, D. A., Li, B., Xiong, X. S., et al. (2019). Underthrusting and duplexing beneath the northern Tibetan Plateau and the evolution of the Himalayan-Tibetan orogen. *Lithosphere* 11 (2), 209–231. doi:10.1130/l1042.1